Biomed Eng Lett (2014) 4:250-257
DOI 10.1007/s13534-014-0150-2

ORIGINAL ARTICLE

# Design Study on Photoacoustic Probe to Detect Prostate Cancer using 3D Monte Carlo Simulation and Finite Element Method

**Sherif Hamdy El-Gohary, Mohamed Kilany Metwally, Seyoung Eom, Seung Hyun Jeon, Kyung Min Byun and Tae-Seong Kim**

Received: 13 August 2014 / Revised: 11 September 2014 / Accepted: 14 Septemer 2014


**Abstract**
*Purpose* In this work, we propose an alternative photoacoustic probe based on transurethral laser illumination to a conventional transrectal photoacoustic imaging system suffering from a high optical absorption at a rectal wall and its surrounding tissues.
*Methods* We validate improved performance of the proposed scheme using 3-dimensional prostate model and analytical calculations such as Monte Carlo simulation and finite element method (FEM). Monte Carlo simulation and FEM are used to find the absorption profiles of photons and the accompanying temperature elevation and pressure signal generation.
*Results* It is found that light source inside the urethra and ultrasound transducer on the rectal wall is an optimal combination to produce a high amplitude in pressure signal and a high signal-to-noise ratio in the reconstructed image. Design study on light source geometry such as beam shape, beam size and gap distance between two light sources is also performed to improve an absorption efficiency at the prostate cancer.
*Conclusions* Our study will be helpful in determining an optimized probe design of photoacoustic imaging system for advancing the detection of prostate cancer.

Sherif Hamdy El-Gohary†, Mohamed Kilany Metwally†, Seyoung Eom, Kyung Min Byun (✉), Tae-Seong Kim (✉)
Department of Biomedical Engineering, Kyung Hee University, Yongin 446-701, Korea
Tel : +82-31-201-3731 / Fax : +82-31-202-1723
E-mail : kmbyun@khu.ac.kr
E-mail : tskim@khu.ac.kr

Seung Hyun Jeon
Department of Urology, Kyung Hee University School of Medicine, Seoul 130-872, Korea

†S. H. El-Gohary and M. K. Metwally contributed equally.

**Keywords** Photoacoustic detection, Prostate cancer, 3-Dimensional Monte Carlo simulation, Finite element method, Transurethral laser illumination, Geometry optimization of light source

## INTRODUCTION

During the last decade, prostate cancer rates have been increasing significantly until it becomes one of the most frequently diagnosed cancers for adult males. Primary risk factors of prostate cancer are known as age, race, and family history [1, 2]. Prostate cancer gets more common with advancing age over 50, when cancer attacks prostate by which cells in the prostate gland become abnormal and begin to grow uncontrollably, thereby forming lesions. Although clinical imaging modalities like ultrasound, computed tomography, and magnetic resonance imaging have been employed for detecting prostate cancer, they suffer from limitations in sensitivity and specificity for screening and finding the cancer in an early stage. As an alternative, optical imaging technique has drawn great interest because it has a potential for offering a high optical contrast between neighboring tissues [3]. Additional advantages of optical imaging include the use of nonionizing radiation and inexpensive instruments compared to other imaging modalities. On the other hand, its major challenge is to overcome the effects of light scattering, which limits penetration depth and achievable imaging resolution. Extremely scattering properties of light waves inside the tissue encourage optical imaging to encompass a wide scope of measurement technique, ranging from laser scanning microscopy of submicron structures to diffuse optical tomography of large volumes of tissue.

In particular, interaction of photons with a tissue can make optical radiation converted into ultrasonic waves which are

suffering less from scattering [4]. Through such a photoacoustic (PA) effect, thermal expansion by absorption of photons inside biomolecules can induce pressure waves and then they relaxes with the propagation of a stress wave in an ultrasound frequency range [5, 6]. By analyzing the ultrasonic waves produced by the absorbing tissues, it is possible to reconstruct their position, size, shape and optical properties [7], which is called photoacoustic imaging (PAI). The PAI is typically limited to a penetration depth of 3-5 cm due to optical absorption and scattering in tissue. Recently, with a help of specialized signal- and image-processing methods, penetration depth, image resolution, and contrast-to-noise ratio can be improved significantly.

In the previous studies, it was reported that PAI can be used as a tool for imaging a prostate cancer. For example, Wang et al. presented a dual-modality imaging system combining PAI with clinical ultrasound imaging to visualize the deep lesions in canine prostate [8]. Yaseen *et al*. used transrectal ultrasound probe and optical fiber bundle for detecting pig's prostate cancer [9]. Also, Bauer et al. worked on mouse samples and insisted that PAI was useful in monitoring the tumor micro-environment by tracking a growth through window chamber [10]. However, the PAI technique still faces some critical challenges, such as how to deliver light waves to target tissue with allowing a high fluence and a minimal invasiveness. Transrectal light illumination combined with ultrasound transducer has been often used to detect the prostate cancer [9], but it is difficult to improve an accuracy in the reconstructed image because a laser power is greatly degraded when penetrating through the rectal wall. On the other hand, we can take an advantage of transurethral probe that was developed for resection and treatment of prostate [11]. Illumination from urethral path will allow the prostate to absorb a light energy more efficiently, therefore producing a larger ultrasound signal for better image reconstruction.

The conversion of optical energy into ultrasonic waves within a biological tissue involves multiple processes including light propagation and absorption, temperature change within the tissue and thermal expansion, and generation of PA signals. In order to understand the whole conversion processes and improve the performance of PAI system, various analytical algorithms, such as finite element method (FEM), have been developed. Rong et al. employed FEM to study an effect of tissue elasticity on the received PA signal and showed that PAI has a potential to differentiate between the malignant and benign tumors based on their contrast in elasticity [12]. The influence of an object size on PAI was explored using FEM and the results obtained were well consistent with the analytical findings by Li *et al*. [13, 14]. FEM-based calculation was also used to optimize the PAI system incorporating a concave mirror for high resolution imaging [15].

In this research, we intend to demonstrate a design study of photoacoustic probe for detecting a prostate cancer. First, light propagation through the prostate tissue is calculated by 3-dimensional (3D) Monte Carlo simulation. Monte Carlo method has been the most widely used to compute a random photon transport in turbid medium that contains absorption and scattering [16, 17]. Second, several PA probe configurations are investigated and parameter optimization is performed. FEM-based calculation is used to obtain the PA signals for individual probe configurations. As a result, we expect that this study will be very useful in understanding and analyzing a photoacoustic effect within the prostate tissue so as to design an optimal photoacoustic probe for diagnosing the prostate cancer more accurately.

## NUMERICAL MODEL AND METHODS

### Numerical model

3D prostate cancer model is illustrated in Fig. 1. The prostate is a small muscular gland beneath urinary bladder. It is shaped like a rounded cone or a funnel with its base pointed superiorly toward the urinary bladder. The prostate surrounds the urethra as it exits the bladder and merges with the ductus deferens at the ejaculatory duct. The proposed 3D model consists of walnut-shaped prostate of $3 \times 3 \times 4$ cm$^3$, urethra with a diameter of 6 mm, bladder surrounding a higher region of prostate, and a small ejaculatory duct of 4 mm in diameter. Fat, muscle and rectal wall with thicknesses of 3, 4, and 2.5 mm are the external layers covering the male reproductive system. Spherical cancer within the prostate has a radius varying with the stage of a prostate cancer.

### 3D Monte Carlo simulation

Monte Carlo method is used to calculate a light propagation

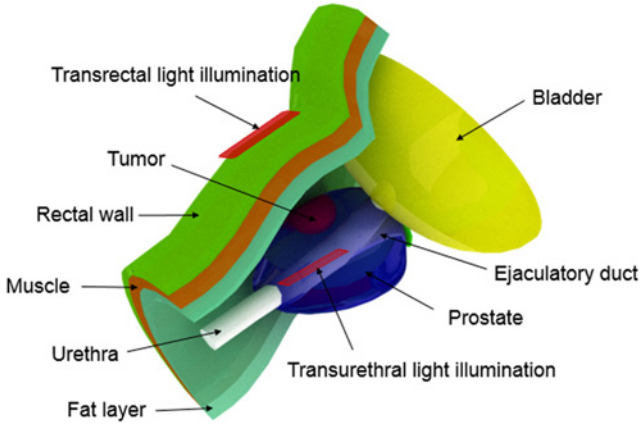


**Fig. 1.** 3D model illustration of the prostate with a tumor and other surrounding tissues.

**Table 1.** Optical properties of prostate, tumor and the neighboring tissues at λ = 1000 nm.

| Tissue | Absorption coefficient $\mu_a$ ($mm^{-1}$) | Scattering coefficient $\mu_s$ ($mm^{-1}$) | Anisotropy g | Refractive index n |
|---|---|---|---|---|
| Rectal wall [23] | 0.330 | 23.08 | 0.93 | 1.36 |
| Muscle [22] | 0.051 | 8.19 | 0.93 | 1.37 |
| Fat [21] | 0.300 | 3.70 | 0.91 | 1.46 |
| Bladder [21] | 0.040 | 11.60 | 0.90 | 1.38 |
| Urethra [9] | 0.024 | 4.33 | 0.65 | 1.40 |
| Prostate [21] | 0.150 | 4.70 | 0.86 | 1.40 |
| Tumor [24] | 0.060 | 12.83 | 0.94 | 1.35 |

within the proposed 3D model. It is a stochastic procedure depending on a random walk, where a photon or a photon package is traced through the tissue until it exits or is terminated due to absorption. By repeating this process for a large number of photon packages, it is possible to obtain the statistics for absorbed photon density. Snell's law at different interfaces may determine the boundary conditions. The procedure describing Monte Carlo simulation can be found in details elsewhere [18].

In this study, 3D Monte Carlo simulations are performed at a specific wavelength of λ = 1000 nm which can produce a high contrast in laser fluence for the prostate and its neighboring tissues [19]. One hundred million photons are randomly generated to guarantee an accuracy in calculations. For the chosen wavelength, the optical properties for prostate and surrounding tissues, such as index of refraction, absorption coefficient, scattering coefficient, and scattering anisotropy are summarized in Table 1. The incident light density is fixed at 15 $mJ/cm^2$ which is below the safety limit to prevent from tissue damage [20].

### Heat distribution

As a result of photon absorption, the temperature at an absorbing tissue changes with time. The change in temperature distribution can be described by the following equation as

$$\rho C\frac{\partial T}{\partial t}-\nabla\cdot(k\nabla T)=H \text{ and } H=\varnothing\mu_a \quad (1)$$

where $\rho$ is the density, $C$ is the specific heat capacity, $k$ is the thermal conductivity, and $T$ is the temperature, respectively. $H$ is the heat generation rate which is a result of multiplication of $\mu_a$, the optical absorption coefficient, and Ø, the fluence rate. The blood perfusion effect is ignored because the laser irradiation time is less than the thermal confinement time [14, 25]. Table 2 presents the thermal properties for the prostate and its neighboring tissues [26].

### Thermal expansion

After the temperature changes within the tissue, a thermoelastic expansion occurs while the temperature rises. This process can be described by the displacement equation below [12].

$$\rho\frac{\partial^2 u}{\partial t^2}-\frac{E}{2(1+\sigma)(1-2\sigma)}\nabla(\nabla\cdot u)-\frac{E}{2(1+\sigma)}\nabla^2 u=\frac{-\beta E}{3(1-2\sigma)}\nabla T \quad (2)$$

where u is the displacement, $E$ is the Young's modulus, $\sigma$ is the Poisson's ratio, and $\beta$ is the thermal expansion. Table 2 includes the mechanical properties of the individual tissues [12, 26].

**Table 2.** Thermal, mechanical and acoustical properties of prostate, tumor and the neighboring tissues.

| Tissue type | Thermal properties | | | Mechanical properties | | | Acoustic properties |
|---|---|---|---|---|---|---|---|
| | Density ($kg/m^3$) | Specific heat capacity (J/kg·k) | Thermal conductivity (W/m·k) | Young's modulus (KPa) | Poisson ratio | Thermal expansion ($K^{-1}$) | Sound speed (m/s) |
| Prostate | 1045 | 3760 | 0.51 | 17 | 0.400 | 1.4e-5 | 1540 |
| Fat | 900 | 2348 | 0.21 | 3.3 | 0.495 | 1.4e-5 | 1450 |
| Bladder | 1035 | 3671 | 0.52 | 10 | 0.490 | 1.4e-5 | 1480 |
| Rectum | 1109 | 3391 | 0.37 | 52 | 0.450 | 1.4e-5 | 1645 |
| Urethra | 1102 | 3306 | 0.46 | 17 | 0.495 | 1.4e-5 | 1480 |
| Muscle | 1090 | 3421 | 0.49 | 10 | 0.490 | 1.4e-5 | 1595 |
| Tumor | 1086 | 3310 | 0.45 | 24 | 0.490 | 8.5e-6 | 1660 |
| Air | 1 | 1003 | 0.03 | 0 | 0.400 | 1.4e-5 | 343 |

### PA signal generation

The acceleration in tumor displacement is converted into an initial pressure ($p$) based on the following conversion equation [27].

$$\frac{\partial p}{\partial n} = -\rho \frac{\partial^2 u_n}{\partial t^2} \tag{3}$$

where $u_n$ is the displacement in the direction of wave propagation. The propagation of initial pressure wave generated at the tumor follows the homogeneous wave equation.

$$\nabla p(r, t) = \frac{1}{v_s^2} \frac{\partial^2 p(r, t)}{\partial t^2} \tag{4}$$

where $v_s$ is the sound speed within the tissue and its values are also provided in Table 2 [26].

The numerical simulation is conducted by FEM simulator [28] and the sparse solver is used to calculate the displacement and the propagating PA pressure wave. For obtaining the PA signals, two linear ultrasound transducers are considered according to the probe configurations. The length of transducer on the rectal wall is assumed to be 2 times the length of the one inside the urethra because urethra is relatively narrower and thinner than rectum.

## RESULTS AND DISCUSSION

### Optimization of probe configuration with light source and ultrasound transducer

Using our 3D prostate model, photon absorption characteristics are compared between transurethral and transrectal approaches when tumor tissue is not present. Fig. 2 shows 2-dimensional (2D) absorption maps by 3D Monte Carlo simulation under identical illumination conditions. It is numerically confirmed that a high absorption is found within the prostate for transurethral case in Fig. 2a while rectal wall, muscle and fat layers lying in a transrectal path absorb most of the incident photons, as shown in Fig. 2b. For that reason, when the photoacoustic probe is loaded on a rectal wall, we can image the prostate cancer only in the vicinity of the rectal wall layer. However, transurethral method has the possibility of imaging the whole volume of the prostate.

To validate an advantage of transurethral approach, a tumor with a radius of 5 mm is inserted at an upper point, 7 mm above the center of urethra. Fig. 3 demonstrates absorption profiles of the prostate with and without a cancer. In Figs. 3a and 3b, for the transrectal cases, since there is no notable difference between the two distribution maps of photon absorption, it is difficult to determine the position and size of a prostate cancer. On the other hand, in the case of transurethral approach, a distinct contrast in absorption feature is shown at the region of spherical tumor. It should also be emphasized that the tumor has a lower absorption than the neighboring tissues due to its relatively smaller absorption coefficient. Nonetheless, the total absorption power within the tumor in transurethral case is about hundred times the value of transrectal case, implying that a higher detection sensitivity in the PA probe is feasible.

Next, we investigate the probe configuration with a laser source and an ultrasound transducer for achieving an improvement in PA signal generation and image reconstruction. We consider three different configurations: (a) transurethral light illumination and pressure sensing, (b) transurethral light illumination and transrectal pressure sensing, and (c) transrectal light illumination and pressure sensing as illustrated in Fig. 4. We do not include a combination of transrectal light

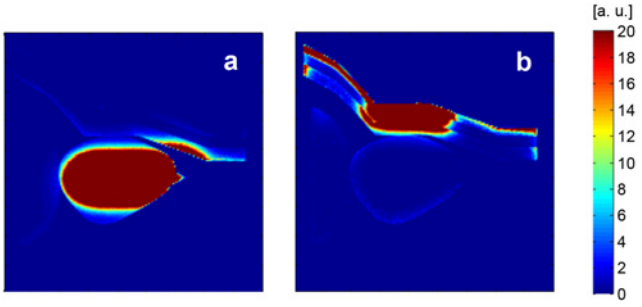


**Fig. 2.** Optical absorption maps based on the 3D prostate model when (a) transurethral and (b) transrectal light illumination is applied.

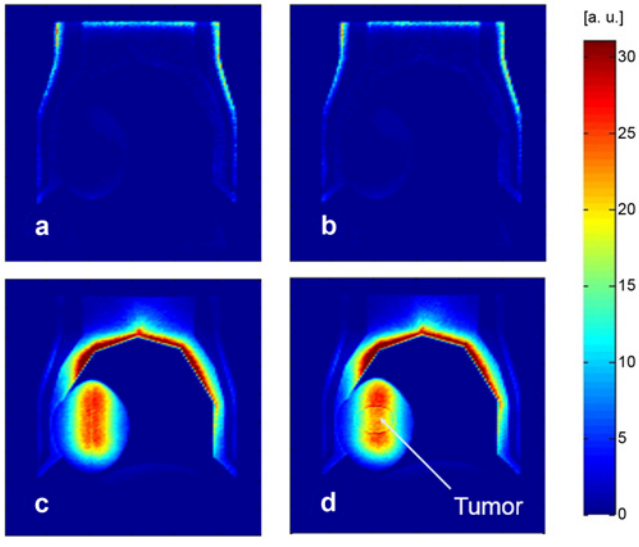


**Fig. 3.** Optical absorption maps for transrectal light illumination to (a) the prostate without a tumor and (b) the one with a tumor and for transurethral light illumination to (c) the prostate without a tumor and (d) the one with a tumor when the tumor has a radius of 5 mm.

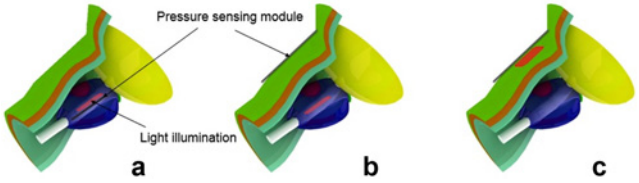


**Fig. 4.** Three different photoacoustic configurations of light illumination and pressure sensing. 1D linear transducer array is assumed to have a length of 40 mm for transurethral pressure sensing scheme and 80 mm for transrectal one.

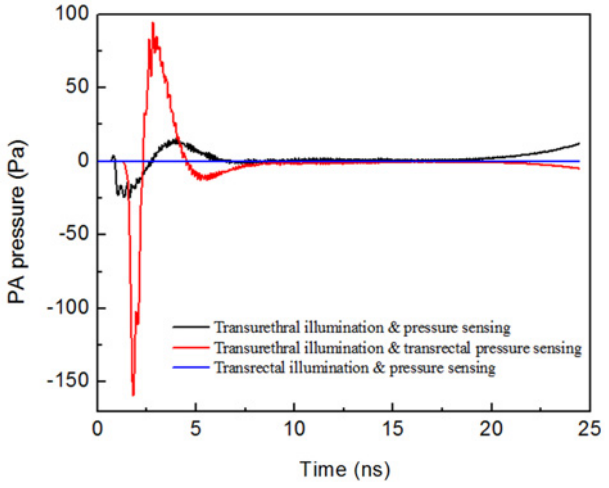


**Fig. 5.** Photoacoustic signals obtained from the tumor with a radius of 5 mm for the three different PAI configurations.

illumination and transurethral pressure sensing because only few photons can be found at the urethra in Figs. 2 and 3. Also, due to the contrast in accessible volume between rectum and urethra, it is also assumed that the length of transducer on the rectal wall is 80 mm and the one inside the urethra is 40 mm. Fig. 5 shows the PA signals calculated for the three probe candidates. Among them, the case of light emission from urethra and pressure signal acquisition at rectal wall exhibits the highest PA signal amplitude of 94.70 Pa. It is attributed to the fact that a greater absorption in the prostate cancer can be achieved by placing laser source within the urethra and the resultant ultrasonic waves can be detected more efficiently by transducer arrays on the rectal wall with a wide viewing angle. For high-resolution image reconstruction of prostate cancer, a longer and wider transducer is demanded to collect the propagating pressure signals as much as possible.

It is interesting to find in Fig. 5 that the obtained PA signals have a negative peak at the first phase, which is contrary to a typical N-shaped pressure signal. It is because the tumor undergoes a shrinkage first and then stretches. This process can be explained by observing a time-varying absorption distribution in the prostate cancer and the surrounding tissues. When light energy reaches the prostate, cancer absorbs less fluence than the surrounding tissues owing to its lower absorption coefficient. Therefore, temperature of the surrounding tissues increases faster and higher than that of the cancer. Such a difference in temperature elevation forces the surrounding tissues to expand and the cancer to shrink during laser illumination. However, at the resting period between laser pulses, temperature of the surrounding tissues starts to decrease, which allows the cancer to expand relatively, leading to a positive pressure peak at the second phase. Also note that asymmetry in negative and positive peaks is associated with an inhomogeneity in temperature profile of a bulky cancer tissue. For the case of illumination from the rectal side, delivered photons at the tumor are very few due to a high absorption of rectal wall, fat and muscle layers and the amplitude of the generated PA signal is thus insignificant and as small as 0.02 Pa.

In order to compare the performance more quantitatively, we perform an image reconstruction using fast Fourier transform algorithm. Fig. 6 illustrates the reconstructed photoacoustic images for the three cases. While the cancer image is not a perfectly spherical and some noise factors are found around the target, combination of a laser source inside the urethra and an ultrasound transducer on the rectal wall

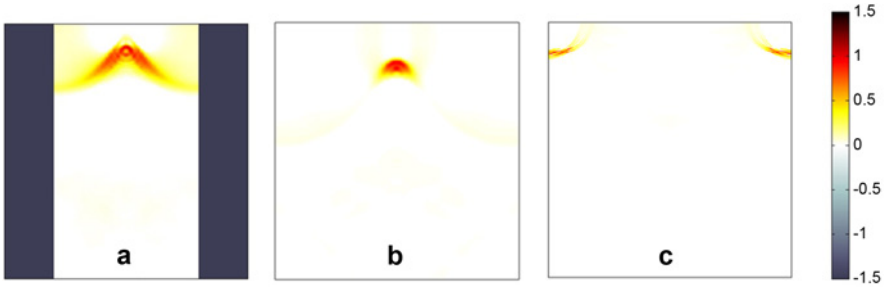


**Fig. 6.** Photoacoustic images reconstructed from (a) transurethral light illumination and pressure signal sensing, (b) transurethral light illumination and transrectal pressure signal sensing, and (c) transrectal light illumination and pressure signal sensing, respectively. The reconstruction image (a) with dark regions is because a length of transducer inside the urethra is assumed to be half a length of the one on the rectal wall.

**Table 3.** Quantitative performance analysis of the pressure signals and the reconstructed images for the three different PAI configurations.

| | Transurethral light illumination and pressure sensing | Transurethral light illumination and transrectal pressure sensing | Transrectal light illumination and pressure sensing |
|---|---|---|---|
| Maximum pressure (Pa) | 15.50 | 94.70 | 0.02 |
| SNR (dB) | 3.06 | 15.94 | 2.26 |

provides the best performance. The optimal photoacoustic probe configuration presents the highest pressure signal of 94.70 Pa and signal-to-noise ratio (SNR) of 15.94 dB. The maximum amplitude in the PA signal and the SNR of the reconstructed images are summarized in Table 3.

**Optimization of light source's geometry**

In this section, we carry an additional design optimization on the geometry of light source to deliver an optical energy more efficiently to prostate cancer. Optimal parameters of laser radiation, such as beam shape, size, and gap distance, are determined based on quantitative metric of normalized density of absorbed photons. Laser source with a wavelength of $\lambda = 1000$ nm is assumed to lie on the center of urethra. Tumor is 7-mm apart from the urethra. All the simulations are performed by 3D Monte Carlo method.

Beam shape

First, beam shape is investigated as the first design parameter of a transurethral laser source. When total area of input laser source is fixed at 32 $mm^2$, rectangular, circular, and ellipsoidal shapes are considered as a candidate for illumination beam. Rectangular and circular light sources consist of two identical elements with an area of 16 $mm^2$. The two elements are in contact each other here, but an influence of gap distance will be demonstrated in the following subsection. Fig. 7 shows that rectangular shape with a dimension of 4 × 8 $mm^2$ yields the highest photon absorption compared with circular and ellipsoidal ones. When tumor size varies from 1 to 5 mm in radius, the enhancement over 25% in photon absorption is provided by the rectangular shape and the overall trends are consistent for all the tumor sizes.

Beam size

Now assuming that the light source has a rectangular shape, the next step is to study an effect of beam size. Because of a narrow urethra with a 6-mm diameter, we vary the total beam size by changing a beam length, while the width is fixed at 4 mm. In Fig. 8, normalized photon density displays a gentle increment because a growing beam length causes illumination area and total illumination energy to increase accordingly. Absorbed photon density is obviously increasing with the beam size and a high absorption over 0.9 is accomplished when the beam length is larger than 17 mm. For the tumor with a radius of 1 mm, while the photon density is relatively slow and somewhat fluctuates, its value almost saturates when the length is over 20 mm. Summarizing the results for rectangular laser illumination, the optimal length with a high photon absorption is determined to be 20 mm while the beam with is fixed at 4 mm.

Gap distance between two light sources

Multiple light sources are required to obtain the images in multiple sites simultaneously. Contrary to single source, double illumination may increase the optical coverage and

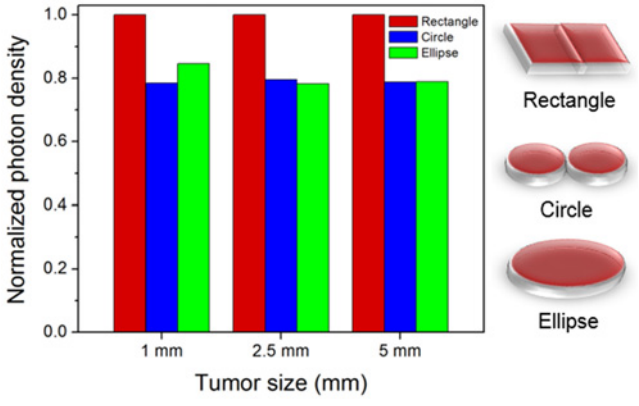


**Fig. 7.** Normalized photon density for tumor absorption for the beam shapes of rectangle, circle, and ellipse.

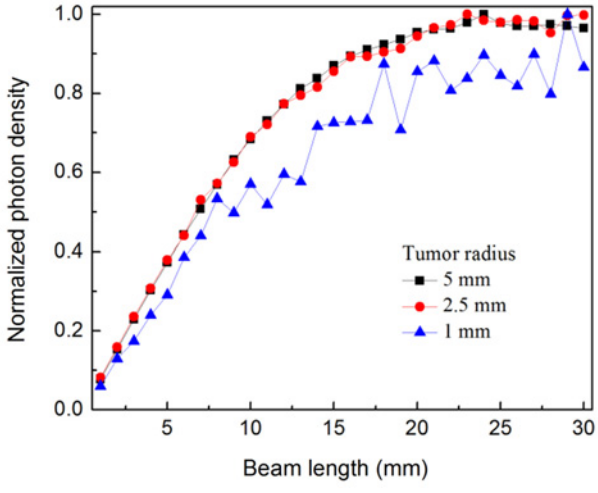


**Fig. 8.** Normalized photon density for the tumor with a radius of 1, 2.5, and 5 mm when the length of rectangular beam increases from 1 to 30 mm as a step of 1 mm. The beam width is fixed at 4 mm.

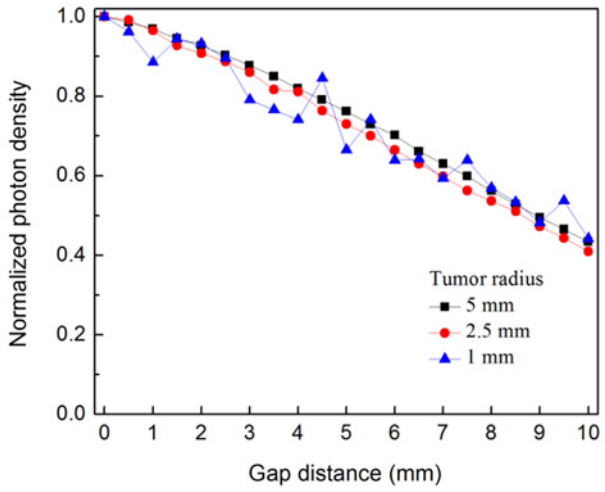


**Fig. 9.** Normalized photon density for the tumor with a radius of 1, 2.5, and 5 mm when the gap distance between two rectangular beams increases from 1 to 10 mm as a step of 1 mm.

thus increase the possibility of finding the cancer. Fig. 9 shows that an increment in gap distance leads to a fair decrease in photon density for absorption. However, a high photon density up to 90% of the maximum value obtained by making two light sources contact each other is maintained until the gap distance is increased to 2.5 mm. By employing a high power laser source below a safety limit, it is expected that we could realize better efficiency in PA signal detection as well as higher SNR in image reconstruction.

## CONCLUSION

In summary, we demonstrated a design study on the photoacoustic detection of prostate cancer based on our 3D prostate model. Monte Carlo simulation and FEM were used to find the absorption profiles of photons and the accompanying temperature elevation and pressure signal generation. Among several probe configurations with light source and ultrasound transducer, transurethral illumination was the most advantageous for efficient light absorption in the prostate cancer and pressure monitoring on the rectal wall showed the highest value in pressure signal amplitude and SNR characteristics. We also found that the PA signal generated by the prostate cancer has an inverted N-shape, which can be attributed to its lower optical absorption than the values of other neighboring tissues.

Further, the 3D prostate model was used to determine optimal geometries of illumination source, such as beam shape, beam size and gap distance between two light sources. From the 3D Monte Carlo calculations for various tumor sizes, rectangular beam exhibited the largest photon absorption over circular and ellipsoidal ones. While the photon deposition was found to be proportional to the length of laser beam, an optimal length was chosen as 20 mm, which can provide a high photon absorption and a minimum invasiveness. An influence of the gap distance between multiple sources was also discussed for achieving a wide optical coverage. Summarizing the simulation results, a pair of rectangular light sources with a length of 20 mm, a width of 4 mm and a gap of 2.5 mm was chosen as an optimum of the PA probe for prostate cancer detection. Our results could give the readers a useful methodology for improving detection accuracy and functional versatility of PAI technique.

## ACKNOWLEDGMENTS

We acknowledge the support of Korea Science and Engineering Foundation (KOSEF) grant funded by the Korean government (MEST) (NSF-2013R1A1A1A05011990).

## CONFLICT OF INTEREST STATEMENTS

El-Gohary SH declares that he has no conflict of interest in relation to the work in this article. Metwally MK declares that he has no conflict of interest in relation to the work in this article. Eom S declares that she has no conflict of interest in relation to the work in this article. Jeon SH declares that he has no conflict of interest in relation to the work in this article. Byun KM declares that he has no conflict of interest in relation to the work in this article. Kim T-S declares that he has no conflict of interest in relation to the work in this article.

## REFERENCES

[1] Siegel R, Naishadham D, Jemal A. Cancer statistics. CA Cancer J Clin. 2013; 63(1):11-30.
[2] Hankey B, Feuer E, Clegg L, Hayes R, Legler J, Prorok P, Ries L, Merrill R, Kaplan R. Cancer surveillance series: Interpreting trends in prostate cancer Part I: Evidence of the effects of screening in recent prostate cancer incidence, mortality, and survival rates. J Natl Cancer Inst. 1999; 91(12):1017-24.
[3] Wang L. Multiscale photoacoustic microscopy and computed tomography. Nat Photonics. 2009; 3(9):503-9.
[4] Pramanik M, Ku G, Li C, Wang L. Design and evaluation of a novel breast cancer detection system combining both thermoacoustic (TA) and photoacoustic (PA) tomography. Med Phys. 2008; 35(6):2218-23.
[5] Kruger R, Reinecke D, Kruger G. Thermoacoustic computed tomography–technical considerations. Med Phys. 1999; 26(9): 1832-7.
[6] Wang L, Zhao X, Sun H, Ku G. Microwave-induced acoustic imaging of biological tissues. Rev Sci Instrum. 1999; 70(9): 3744-8.
[7] Xu M, Wang L. Photoacoustic imaging in biomedicine. Rev Sci

Instrum. 2006; doi:10.1063/1.2195024.
[8] Wang X, Roberts W, Carson P, Wood D, Fowlkes J. Photoacoustic tomography: a potential new tool for prostate cancer. Biomed Opt Express. 2010; 1(4):1117-26.
[9] Yaseen M, Ermilov S, Brecht H, Su R, Conjusteau A, Fronheiser M, Bell B, Motamedi M, Oraevsky A. Optoacoustic imaging of the prostate: development toward image-guided biopsy. J Biomed Opt. 2010; doi:10.1117/1.3333548.
[10] Bauer D, Olafsson R, Montilla L, Witte R. 3-D photoacoustic and pulse echo imaging of prostate tumor progression in the mouse window chamber. J Biomed Opt. 2011; doi: 10.1117/1.3540668.
[11] Rassweiler J, Teber D, Kuntz R, Hofmann R. Complications of transurethral resection of the prostate (TURP)—Incidence, management, and prevention. Eur Urol. 2006; 50(5):969-79.
[12] An R, Luo X, Shen Z. Numerical simulation of the influence of the elastic modulus of a tumor on laser-induced ultrasonics in soft tissue. Appl Opt. 2012; 51(32):7869-76.
[13] An R, Luo X, Shen Z. Numerical and experimental investigation of the influence of tumor size on laser-induced ultrasonics in soft tissue. Laser Phys. 2014; 24(4):045604.
[14] Li C, Wang L. Photoacoustic tomography and sensing in biomedicine. Phys Med Biol. 2009; 54(19):R59-97.
[15] Wang Z, Ha S, Kim K. Photoacoustic design parameter optimization for deep tissue imaging by numerical simulation. Proc SPIE Photons Plus Ultrasound: Imaging and Sensing. 2012; doi:10.1117/12.912973.
[16] Xie Z, Wang L, Zhang H. Optical fluence distribution study in tissue in dark-field confocal photoacoustic microscopy using a modified Monte Carlo convolution method. Appl Opt. 2009; 48(17):3204-11.
[17] Periyasamy V, Pramanik M. Monte Carlo simulation of light transport in tissue for optimizing light delivery in photoacoustic imaging of the sentinel lymph node. J Biomed Opt. 2013; doi: 10.1117/1.JBO.18.10.106008.
[18] Popov A, Priezzhev A. Laser pulse propagation in turbid media: Monte Carlo simulation and comparison with experiment. Proc SPIE 5068. 2003; doi:10.1117/12.518792.
[19] Ren S, Chen X, Wang H, Qu X, Wang G, Liang J, Tian J. Molecular optical simulation environment (MOSE): A platform for the simulation of light propagation in turbid media. PloS One. 2013; 8(4):e61304.
[20] Charschan S, Rockwell B. Update on ANSI Z136.1. J Laser Appl. 1999; 11(6):243-7.
[21] Vo-Dinh T. Biomedical photonics handbook. 1st ed. Boca Raton: CRC Press; 2003.
[22] Boas D, Pitris C, Ramanujam N. Handbook of biomedical optics. 1st ed. Boca Raton: CRC Press; 2011.
[23] Agrba P, Kirillin M, Abelevich A, Kamensky V. Mechanical compression for biotissue image enhancement in optical coherence tomography. Proc SPIE 7547. 2010. doi: 10.1117/12.853436.
[24] Svensson T, Andersson-Engels S, Einarsdóttír M, Svanberg K In vivo optical characterization of human prostate tissue using near-infrared time-resolved spectroscopy. J Biomed Opt. 2007; 12(1):014022.
[25] Telenkov S, Mandelis A, Lashkari B, Forcht M. Frequency-domain photothermoacoustics: Alternative imaging modality of biological tissues. J Appl Phys. 2009; doi: 10.1063/1.3116136.
[26] McIntosh R, Anderson V. A comprehensive tissue properties database provided for the thermal assessment of a human at rest. Biophys Rev Lett. 2010; 5(3):129-51.
[27] Metwally M, Han H, Jeon H, Khang G, Kim T. Influence of the anisotropic mechanical properties of the skull in low-intensity focused ultrasound towards neuromodulation of the brain. Conf Proc IEEE Eng Med Biol Soc. 2013l; 2013:4565-8.
[28] ANSYS® Academic Research Home Page. http://www.ansys.com. Accessed 25-Sep-2014.